Available online at www.sciencedirect.com
SCIENCE DIRECT®
Experimental Thermal and Fluid Science 29 (2004) 41–52
Experimental Thermal and Fluid Science
www.elsevier.com/locate/etfs

On the effects of lateral wall oscillations on a turbulent boundary layer

Pierre Ricco *, Shengli Wu [1]

Mechanical Engineering Department, The University of Texas at Austin, 1 University Station C2200, Austin, TX 78712, USA

Received 21 June 2003; accepted 27 January 2004

Abstract

A turbulent boundary layer modified by spanwise wall oscillations is experimentally studied in a water channel by means of hot-film anemometer and laser Doppler velocimeter. The primary goal is to confirm and extend previous experimental and numerical results concerning the modifications induced by the lateral cyclic wall motion on wall-bounded turbulent flows. A correction is applied to the hot-film data acquired in the very proximity of the wall because of the spanwise velocity component produced by the wall movement, which erroneously alters the longitudinal velocity measurements and leads to lower values of drag reduction. It is found that the excited boundary layer shows a character which is sustained in time with stationary time-averaged quantities. The mean streamwise friction at the wall and all the most relevant turbulence statistics are attenuated by the oscillation, thus confirming the oscillating wall as an effective vehicle for producing a drag reduction effect. Furthermore, the evolution of the skin-friction coefficient along the oscillating wall and its readjustment downstream of the moving section are also investigated. The length of the spatial transient from the beginning of the oscillating wall is at least double the distance downstream of the moving plate at which the turbulent flow relaxes back to its original unperturbed state. Experiments reveal that the drag reduction properties of the oscillating wall technique are not influenced by the variation of the Reynolds number, at least for the cases tested, i.e. for $Re_\theta \leqslant 1400$.

Keywords: Drag reduction; Turbulent boundary layer; Spanwise wall oscillation

1. Introduction

The present work is intended to further investigate the changes on a turbulent boundary layer given by a sinusoidal spanwise motion of the wall. In the last decade, a few research groups have focused their attention on this flow problem in planar and cylindrical geometries, both via direct numerical simulations [1–7] and experimentally [8–12]. A recent appraisal of the effects of wall oscillation on turbulent flows has been published by Karniadakis and Choi [13], where connection is made with similar drag reduction techniques, such as the excitation of the near-wall flow by transverse travelling waves [14].

General agreement exists on the fact that wall oscillations of appropriate amplitude and frequency inhibit the turbulence activity, thereby guaranteeing a persistent skin-friction reduction. According to many authors, the mean streamwise velocity gradient at the wall can be reduced by as much as 40% [1–4,7,10]. Preliminary numerical investigations by Baron and Quadrio [2] for a plane channel flow and by Quadrio and Sibilla [3] for a pipe flow oscillating about the longitudinal axis indicate that the global energy balance, considering the external power needed to move the wall against the frictional resistance of the fluid, might be positive and comparable to the energy saving of other drag reduction techniques, such as riblets [15].

Since the first study by Jung et al. [1], the action of the wall has been correctly recognized as being effective in the suppression of the burst-sweep activity, although the

* Corresponding author. Present address: Department of Mathematics, Imperial College, 180 Queen's Gate, London SW7 2BZ, UK. Tel.: +44-20-7594-8555; fax: +44-20-7594-8517.
E-mail address: pierre.ricco@imperial.ac.uk (P. Ricco).
URL: http://www.ma.ic.ac.uk/~par.
[1] Present address: Parsons Energy & Chemicals Inc., 5 Greenway Plaza, Houston, TX 77079, USA.

0894-1777/$ - see front matter © 2004 Elsevier Inc. All rights reserved.
doi:10.1016/j.expthermflusci.2004.01.010

Nomenclature

B	constant in "log-law" expressed by Eq. (2) ($=5.0$), dimensionless
C_f	skin-friction coefficient ($=2\tau_w/(\rho U_\infty^2)$), dimensionless
D	wall spanwise displacement given by Eq. (1), m
D_m	peak-to-peak displacement of the wall oscillation, m
h	channel height, m
K_1, K_2	Jorgensen coefficients, dimensionless
R_{uv}	correlation coefficient ($=\overline{uv}/u'v'$), dimensionless
Re_θ	Reynolds number based on θ ($=U_\infty\theta/\nu$), dimensionless
Re_τ	Reynolds number for channel flow based on u_τ and $h/2$, dimensionless
T	period of the wall oscillation, s
U, V, W	mean streamwise, vertical and spanwise velocity, m/s
U_{act}	actual mean streamwise velocity, m/s
U_{meas}	measured mean streamwise velocity, m/s
U_{oscill}	mean streamwise velocity in oscillating wall configuration, m/s
U_{stat}	mean streamwise velocity in stationary wall configuration, m/s
u_τ	friction velocity for stationary wall configuration ($=\sqrt{\tau_w/\rho}$), m/s
$u_{\tau,o}$	friction velocity for oscillating wall configuration ($=\sqrt{\tau_{w,o}/\rho}$), m/s
U_∞	local free-stream velocity, m/s
u', v'	r.m.s. of streamwise and vertical velocity, m/s
$\overline{uv}$	turbulent shear stress divided by ρ, m^2/s^2
$\overline{uv}\partial U/\partial y$	turbulent kinetic energy production term, m^2/s^3
$\partial(\overline{uv}U)/\partial y$	turbulent kinetic energy transport term, m^2/s^3
W_m	maximum spanwise wall velocity ($=\pi D_m/T$ from Eq. (1)), m/s
x, y	streamwise and vertical direction, m
δ	boundary layer thickness, i.e. y location where U is 99% of U_∞, m
δ_s	thickness of Stokes layer ($=\sqrt{4\pi\nu T}$), m
Δl	width of gap between stationary false floor and moving section, m
θ	boundary layer momentum thickness, m
κ	constant in "log-law" expressed by Eq. (2) ($=0.41$), dimensionless
ν	kinematic viscosity of the fluid, m^2/s
ρ	density of the fluid, kg/m^3
τ_w	mean streamwise wall-shear stress, $kg/(m\,s^2)$
$\tau_{w,o}$	mean streamwise wall-shear stress for oscillating wall case, $kg/(m\,s^2)$
$+$	indicates quantity normalized by inner variables, i.e. by u_τ and ν

comprehension of the flow mechanisms brought about by the oscillating motion was still at its early stages at that time. Laadhari et al. [8] were the first ones to postulate that the reduction of turbulence level is caused by the disruption of the coherent interactions between the quasi-streamwise vortices and the underlying low-velocity streaks. In the perturbed boundary layer, these structures are now shifted relatively to each other in the spanwise direction. Bursts and sweeps are consequently suppressed for the sublayer structure is more homogenized and less eager to erupt to the buffer region and beyond. In the spirit of these pioneering investigations, the interest on the subject has amply grown in the past few years, and the picture of the physical modifications induced by the wall movement has been subsequently supported, confirmed and expanded [2,3,6,9,16]. Choi et al. [5] have recently assured the existence of an optimal period of oscillation for a fixed maximum wall velocity, and proposed a scaling quantity for drag reduction, function of both the oscillatory parameters.

We have devoted our attention to the oscillating-wall flow motivated by the remarkable fact that such a simple modification may induce a net energy gain without the need of feedback laws or small-scale actuators. Our interest toward such a method for wall turbulence control has been also fostered by the conviction that a profound understanding of the mechanisms characterizing such a flow can be of notable importance for the implementation of similar energy-saving techniques. In this regard, we mention the study by Berger et al. [17] who employed a spatially or temporally oscillating, spanwise-oriented Lorentz force in the near-wall region of a turbulent flow of an electrically conducting fluid. However, it must be remarked that, contrarily to the oscillating wall, the technique proposed by Berger et al. [17] shows an extremely unfavorable net energy balance, being the ratio between the power required to generate the force and the power saved as high as $\mathcal{O}(1000)$.

The first aim of the present research work is to measure the amount of drag reduction along the streamwise direction on the moving plate and downstream of it in order to investigate the behavior of the spatial transient. None of the previous works on the subject has heretofore addressed the problem of the streamwise evolution of wall friction, if exception is made for a preliminary investigation by Choi et al. [10]. They underlined the importance of such an analysis and surmised that the moving section could have been not

long enough to measure the maximum drag reduction attainable through spanwise wall oscillations.

A thorough understanding of the spatial evolution of friction along the oscillating wall is not only interesting per se, but it also allows determining the correct downstream position to conduct the velocity measurements along the wall-normal direction. Indeed, an experimental campaign of a turbulent flow spatially adjusting to a new statistically steady regime should be performed at a location where the spatial transient has fully elapsed and the new state has established.

The dual process of the spatial transient, namely the temporal evolution of the friction coefficient from the beginning of the oscillation at a fixed spatial location, has been recently studied by Quadrio and Ricco [6] by means of highly accurate direct numerical simulations. The temporal transient is obviously also present in experiments, but it does not influence the velocity measurements as long as data are acquired after this initial time interval, which was estimated by Quadrio and Ricco [6] being $\mathcal{O}(1000)$ viscous time units even for the longest time evolutions. Among the experimental studies, only Choi [12] briefly mentioned the existence of a temporal transient claiming that it becomes negligible after one cycle of oscillation, regardless of the period and amplitude of the sinusoidal motion.

Measurements along the normal direction were conducted by means of single-component hot-film anemometer and laser Doppler velocimeter (LDV) systems in the viscous sublayer and in the lower part of the buffer region in order to determine the amount of drag reduction, whilst a two-component LDV system was employed to acquire data along the remaining part of the boundary layer. The hot-film velocity measurements were biased by the spanwise-oscillating velocity component given by the wall movement, so that a correction was applied to determine the amount of drag reduction. Amongst the previous experimental works, only Choi [12] showed a similar correction to the velocity measurements. We also present the distribution of turbulent kinetic energy (TKE) production and transport terms, and we address the issue of the dependence of drag reduction on the Reynolds number.

The layout of the article is as follows. The next section outlines the laboratory apparatus and the experimental techniques, while the drag reduction results, the turbulent statistics and the influence of the Reynolds number are presented and discussed in Section 3. Finally, conclusions are contained in the last section.

2. Experimental apparatus and procedure

The experiments and data analysis were performed at the Turbulence and Turbine Cooling Research Laboratory in the Mechanical Engineering Department at The University of Texas at Austin. The laboratory equipment consisted of a low-speed recirculating water channel, hot-film anemometer and laser Doppler velocimeter systems.

2.1. Water channel and oscillating wall

The experiments were all performed in a closed-loop channel through which water was driven by two pumps in parallel. The channel facility, shown in Fig. 1, allowed

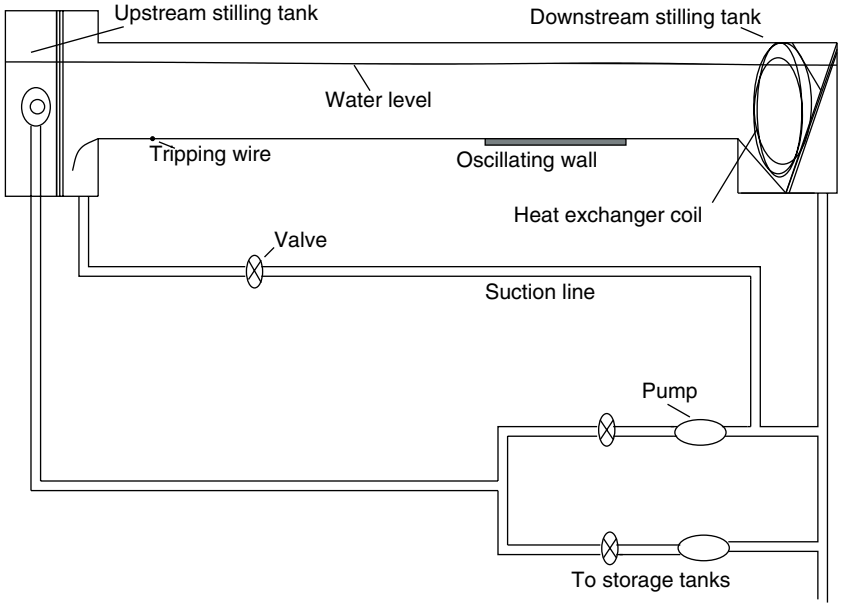

Fig. 1. Schematic of water channel facility.

achieving the desired free-stream velocities of nominally 0.18 m/s with one pump and 0.3 m/s with two pumps. The channel was free-surfaced and had a test section of 5 m long, 0.5 m wide and 0.3 m deep. It was made of 12.7-mm-thick cast acrylic sheets. A 3-mm diameter rod was located at a streamwise position of 0.5 m to trip the boundary layer flow. Water flowed from a first stilling tank on a false floor, where the oscillating wall mechanism was installed at a streamwise position of 3.5 m from the inlet of the test section. The Reynolds numbers were $Re_\theta = 500$, 950 and 1400. Turbulence statistics were measured for the case dictated by $Re_\theta = 1400$, in which the boundary layer thickness δ measured about 60 mm and $U_\infty = 0.18$ m/s. The water level for the experiments was 0.2 m from the false floor surface. After the moving section, the flow proceeded toward a second stilling tank and then to the piping system. Water was filtered to a submicron level through a two-stage process for all the experiments. For hot-film anemometer measurements, water was deaerated by heating to 60 °C after filtering.

The oscillating section was 660 mm long × 450 mm wide and was mounted on a pair of linear bearings. The motion was given by a crank-slider mechanism connected to a Compumotor M106-178 stepping motor regulated by an IBM PC-AT computer. The period of oscillation was imposed electronically, whilst the lateral excursion was fixed manually. The spanwise wall displacement D followed a sinusoidal function of time:

$$D = \frac{D_m}{2} \sin\left(\frac{2\pi t}{T}\right), \tag{1}$$

and the actual wall motion presented an estimated 3% deviation from the ideal curve. The wall oscillation can also be defined by the maximum wall velocity W_m, which is related to the other oscillation parameters by the following: $W_m = \pi D_m/T$. The interested reader should refer to [18] for a more complete description of the experimental facility.

2.2. Hot-film anemometer and laser Doppler velocimeter

A TSI model 1261-10W miniature hot-film boundary layer probe with a A.A. Lab Systems model AN-1003 constant-temperature anemometer was used for single-component hot-film measurements. The probe was made of platinum and the substrate of quartz. It had dimensions of 0.025 mm ($\approx 0.3\nu/u_\tau$ for $Re_\theta = 1400$) in diameter and 0.5 mm ($\approx 5\nu/u_\tau$) in length. The hot film had a maximum frequency response of 200 kHz and it was operated at an overheat of 20 °C. The overheat ratio was $R_f/R_a = 1.05$, where R_f is the electric resistance of the sensor and R_a is the resistance under ambient conditions (temperature coefficient of resistance $\alpha = 0.0024$ $°C^{-1}$). The effects of substrate conduction were considered negligible, as the probe had a cylindrical shape and it was operated in water [19,20].

All the measurements were conducted by inserting the sensor from the open surface. Four samples, each 3-min-long and of 36,000 data points, were acquired, resulting in a sampling frequency of 200 Hz ($\sim 2.9u_\tau^2/\nu - t^+ = 0.34$ for the stationary wall case and $\sim 4.4u_\tau^2/\nu - t^+ = 0.23$ for the oscillating wall case with the maximum drag reduction of 32%). This frequency was proved to be adequate to accurately resolve the smallest time scales, as recently shown by Khoo et al. [21]. Indeed, the Kolmogorov time scale in the viscous sublayer is $t^+ \approx 1$ [22]. The hot-film anemometer was used for measurements at $3 < y^+ < 10$ (between 0.3 and 1 mm, approximately) and along the surface of the oscillating surface and downstream of it.

A two-component laser Doppler velocimeter system positioned at the side of the water channel at a downstream location corresponding to the oscillating wall and perpendicular to the streamwise direction of the flow was used to measure mean, r.m.s fluctuations and correlations of streamwise and vertical components of velocity. It consisted of a backscatter TSI model 9100-10 3W argon-ion laser, a 3.75X beam expander, a 450-mm focusing lens and a Bragg cell frequency shifter used to determine the wall-normal velocity component. The LDV was mounted on a traverse table that offered a resolution of 0.002 mm ($\approx 0.02\nu/u_\tau$) in the three orthogonal directions. The ellipsoidal probe volume given by the intersection of the beams had dimensions of 0.07 mm in diameter ($\approx 0.7\nu/u_\tau$) and 0.5 mm in length ($\approx 5\nu/u_\tau$). Five samples, each 2-min-long and of 24,000 data points, were collected at each measuring location, which results in a sampling frequency of 200 Hz. Owing to limitations due to high noise-to-signal ratio, these LDV measurements could only be made at the lowest location of $y^+ \approx 10$ from the wall surface.

A fiber-optic single-component LDV system positioned on top of the channel was also used to measure the mean streamwise velocity component very close to the wall ($y^+ < 10$). A Lexel argon-ion laser gave the light source input to a fiber optic, which transmitted the beam to the LDV optics. Scattered light from the probe volume was collected by the TSI acquisition system positioned at the side of the water channel. By using the side-scatter mode, it was possible to obtain a good quality signal in the viscous sublayer and in the lower part of the buffer region, due to the elimination of laser flare which overwhelmed the fiber-optic LDV signal in the back-scatter mode. Due to the relatively bigger size of the probe volume, a smaller pinhole of 0.2 mm in diameter for the photo-detector in the side-scatter collection was also used to limit the detecting region to 1.5 viscous units at maximum and to reduce the uncertainty of the velocity measurement. The sampling frequency for the

top LDV system was between 20 and 40 Hz, hence lower than the side-LDV for the use of the very small pinhole of 0.2 mm in diameter. Four samples, each 3.5–6.5-min-long and of 8000 data points, were acquired for each measuring location. A "binning" and a smoothing process were applied to the LDV signal in order to obtain a uniform time history and to eliminate undesired noise. The binning process consisted in selecting the bin time size ($t^+ \approx 1$) and in calculating the time average of velocity in each bin. In case of a bin not containing any data, the velocity was estimated by averaging the values of velocity of the two closest bins. The noise-removing smoothing process consisted in substituting the velocity of the bin with the average velocity of the closest bins and itself. For side-LDV experiments, the wall-normal location of measurement was estimated by first carefully crossing the laser beams at the wall surface and by then moving the probe volume vertically to the desired vertical height. For hot-film and top-LDV experiments, the actual height of the detecting position was determined by measuring the mean streamwise velocity in the viscous sublayer, where $U^+ = y^+$ [23].

2.3. Uncertainty analysis

Guidelines for uncertainties are tabulated in Table 1. These values refer to measurements in the near-wall region where velocity gradients and hence uncertainties are highest. Note that the percentage uncertainty of drag reduction refer to the drag reduction value itself, namely, for example, an uncertainty value of ±7.5% for 31% drag reduction translates into 31% ± 2.3%. The analysis for the LDV individual velocity measurements accounted for the precision errors due to the calculation of the angle of the laser beams' intersection and of the Doppler frequency, whereas the bias error related to the frequency was assumed negligible. Uncertainties related to ensembled-based quantities for both LDV and hot-film measurements were calculated by a multiple-sample technique with a 95% confidence level.

As shown in Section 3.2, the turbulence statistics for the uncontrolled case compare well with the DNS results at $Re_\theta = 1410$ by Spalart [24] and with the high-resolution LDV measurements at $Re_\theta = 1430$ by DeGraff and Eaton [25].

Table 1
Uncertainty guidelines

Quantity	Uncertainty (%)
LDV U	±1.5
Hot-film U	±4.5
LDV u'	±2
Hot-film u'	±3
LDV v'	±3
LDV $\overline{uv}$	±10
Drag reduction—hot-film	±11.5
Drag reduction—top LDV	±7.5

The friction velocity for the fixed-wall case was measured by fitting the velocity data with the logarithmic law of the wall (or "log-law" as named in Fig. 4):

$$U^+ = \frac{1}{\kappa}\ln y^+ + B, \tag{2}$$

where $\kappa = 0.41$ and $B = 5.0$. This value is $u_\tau = 0.0083$ m/s and is only 2% different from $u_\tau = 0.008137$ m/s given by the following correlation [26]:

$$C_f = \frac{2\tau_w}{\rho U_\infty^2} = 0.025 Re_\theta^{-0.25},$$

where $Re_\theta = 1400$ and $U_\infty = 0.18$ m/s.

2.4. Drag reduction measuring technique

The mean streamwise velocity component was measured in the viscous sublayer in order to determine the reduction of the wall-shear stress. This procedure was also adopted by Choi et al. [10] and Trujillo et al. [9]. According to Durst et al. [23], the velocity in the sublayer does not exactly follow a linear trend, showing a maximum 4% deviation at $y^+ = 5$. However, the net effect of the non-linearity on the final result was assumed negligible, in as much as drag reduction was calculated from velocity measurements at wall-normal locations $y^+ < 5$, where the maximum deviations of the velocity profile from the linear distribution are of only 1.1% at $y^+ = 3$ and of 2% at $y^+ = 4$.

In theory, this procedure is very useful because it allows an estimate of the wall stress reduction regardless of the position of the probe near the wall, as long as it is located well inside the "linear" viscous sublayer, namely at $y^+ = 4$ at maximum. Unfortunately, the hot-film anemometer experiments did not mirror the expected results owing to the spanwise component of the velocity given by the wall oscillation which influenced the heat transfer from the probe and altered the measurement. Fig. 2 presents the behavior of the percentage of mean streamwise velocity deficit due to the wall oscillation

$$U_{RID}(\%) = 100\left(1 - \frac{U_{oscill}}{U_{stat}}\right) \tag{3}$$

at different y^+ positions. Data clearly show that the motion of the wall has a greater influence on the hot-film measurements the closer is the probe located to the wall. This is expected since the spanwise velocity is higher at lower wall-normal locations.

The following correction procedure was then applied to the measured mean velocity data to account for the influence of the spanwise motion. The single hot-film anemometer used for the present research was sensitive to the three velocity components, according to the Jorgensen relation given by [27]:

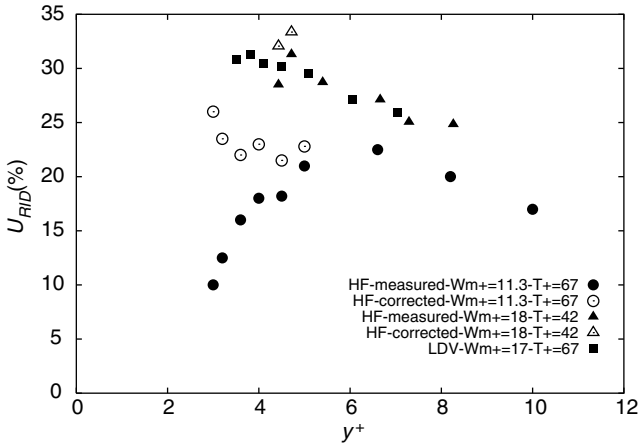

Fig. 2. Mean velocity reduction expressed by Eq. (3) as function of y^+ at $x/\delta = 6.4$. Hot-film measurements are indicated by HF and top-LDV measurements by LDV.

$$U_{\text{meas}}^2 = U_{\text{act}}^2 + (K_1 W)^2 + (K_2 V)^2,$$

which can be simplified to:

$$U_{\text{meas}}^2 = U_{\text{act}}^2 + (K_1 W)^2,$$

since $V \sim 0$. $K_1 = 0.5$ for the hot-film probe used and was assumed constant, following the analysis by Choi [12]. The laminar Stokes solution was used to estimate W, since the spanwise velocity component closely follows the analytical profile, as shown in [3,5,6,28]. The actual streamwise velocity was then calculated averaging over time the following:

$$U_{\text{act}}(y,t) = \sqrt{(U_{\text{meas}}(y,t))^2 - (K_1 W(y,t))^2}.$$

The corrected data are shown in Fig. 2.

The friction velocity for the oscillating-wall case can then be estimated by averaging the corrected streamwise mean velocity gradients at locations $y^+ < 5$, as follows:

$$u_{\tau,\text{o}} = \sqrt{\frac{\tau_{\text{w,o}}}{\rho}} = \sqrt{\frac{\nu}{N}\sum_{i=0}^{N}\left(\frac{U_{\text{act},i}}{y_i}\right)}, \tag{4}$$

where $\tau_{\text{w,o}}$ is the local streamwise wall-shear stress and N is the number of wall-normal measuring locations. The amount of drag reduction is also readily determined:

$$\begin{aligned}\text{DR}(\%) &= 100\left(1 - \left(\frac{u_{\tau,\text{o}}}{u_\tau}\right)^2\right) \\ &= 100\left(1 - \frac{\frac{\nu}{N}\sum_{i=0}^{N}\left(\frac{U_{\text{act},i}}{y_i}\right)}{u_\tau^2}\right).\end{aligned}$$

As notable in Fig. 2, it is desirable not to conduct hot film measurements lower than $y^+ = 3.5$–4 because of the much higher influence of the spanwise velocity component.

Moreover, we note that the velocity deficit shows a decaying behavior for $y^+ > 5$. This trend is obviously not related to the bias due to the spanwise component, but it expresses the character of the modified boundary layer in the buffer region. As it will be discussed later, the velocity ratio will then decrease to zero at a vertical position of $y^+ \approx 30$, where no reduction of the streamwise velocity is observed. Choi [12] also employed a similar technique to account for the effect of the spanwise velocity and showed that the maximum error was only 4%, hence smaller than in the present case, probably on account of the smaller Jorgensen coefficient ($K_1 = 0.2$) of the probe used.

Mean velocities were also measured in the viscous sublayer with the top LDV system to calculate drag reduction. Obviously, this technique did not need the correction due to the spanwise component of velocity. It was anyway necessary to accurately position the probe volume in the "linear" sublayer or at the edge of it ($y^+ < 5$). This is confirmed by measurements of mean velocity reduction for $T^+ = 67$ and $D_{\text{m}}^+ = 360$, as displayed in Fig. 2. The velocity reduction remains fairly constant at $\sim 31\%$ for $y^+ \leqslant 4$, and starts to diminish at higher locations. A 27% velocity reduction was observed at $y^+ \approx 6$ and 26% at $y^+ \approx 7$.

3. Results and discussion

3.1. Drag reduction as function of streamwise coordinate

The streamwise variation of the drag reduction from the foremost edge and downstream of the plate for $T^+ = 67$, $D_{\text{m}}^+ = 240$ ($W_{\text{m}}^+ = 11.3$) and $Re_\theta = 1400$ is shown in Fig. 3.

A fast response to the oscillating motion lies within a distance of 1δ, where the wall stress reduction abruptly increases to 17%. After this location, the turbulent flow is still evolving to a new equilibrium state, but in a less pronounced way, so that a 7–8% increase is observed from 1 to $\sim 3\delta$, reaching a 23% drag reduction at $x/\delta \approx 3$. After this location, the effect of the oscillation adjusts to 23–24%. No measurements were conducted in the $0 < x/\delta < 0.3$ range since the flow might have been influenced by disturbances produced by a gap of about $\Delta l^+ \approx 20$ existing between the oscillating plate and the false floor located upstream. Extrapolating the drag reduction trend for $x/\delta < 1$, it seems that the energy-saving effect dies out at the beginning of the moving wall, but experiments have not been performed upstream of the wall to support this theory. Fig. 3 also shows that the drag reduction measurements by Trujillo et al. [9] at $x/\delta = 0.8$, 4.2 and 7.2 well compare with the ones of the present study.

The velocity measurements on the moving surface were corrected because of the spanwise component of

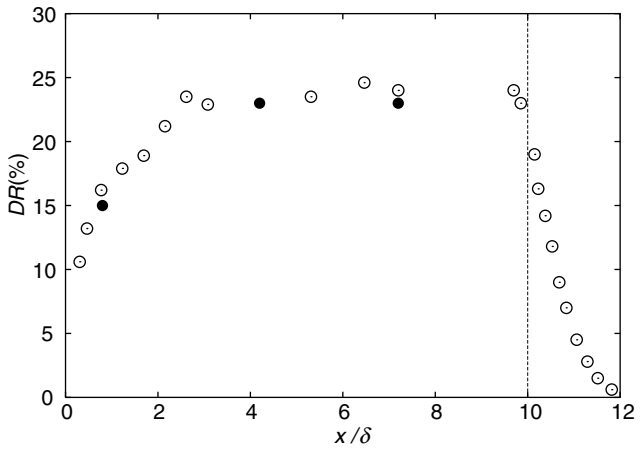

Fig. 3. Drag reduction (DR) as function of streamwise coordinate for $T^+ = 67$ and $D_m^+ = 240$ ($W_m^+ = 11.3$) (white circles). Black circles indicate data by Trujillo et al. [9] and straight line denotes rearmost edge of moving wall.

the velocity, whereas no correction was applied to measurements conducted downstream of the oscillating plate. The spanwise velocity might have slightly altered the measurements performed very close to the rearmost edge of the plate, but this influence was not considered to be relevant to apply the correction.

Downstream of the plate a very smooth exponent-like behavior is observed, indicating the decaying of the oscillation effect. Similarly to the transient response at the beginning of the plate, the steeper gradients are detected as soon as the flow passes the rearmost edge, where as much as 15% drop occurs at a location of 0.3δ downstream of the wall. For the same reason previously mentioned, no measurements were performed very close to this point. No drag reduction has been detected once the boundary layer develops after a distance of 2δ from the plate, location at which the flow retains its original character.

It is worth mentioning that the decrease of drag reduction is about two times more rapid than the transient from the beginning of the plate, where it takes about $3-4\delta$ to reach the new excited regime. This peculiar behavior seems to preclude a more efficient way of forcing the boundary layer, namely with a set of spanwise-oscillating belts separated by sections of stationary wall. This would reduce the power spent to excite the flow, but would also more significantly diminish the power saved on account of the lengthy initial transient.

The velocity measurements along the vertical direction were conducted at $x/\delta = 6.4$, location which is about double the length of the initial spatial transient for $T^+ = 67$ and $D_m^+ = 240$ ($W_m^+ = 11.3$). This position was chosen in order to be free from any transitional effects, which might bias the measurements. It must be remarked that measurements with the highest maximum wall velocity ($W_m^+ = 22$) might have been performed very near the end of the spatial transient given by these oscillatory conditions, for Quadrio and Ricco [6] pointed out that, whilst the period does not significantly affect the transient evolution, doubling W_m could double the length of the spatial transient. Experiments were not conducted farther downstream along the moving wall lest the flow beyond the end of moving section might influence the upstream perturbed flow.

Choi et al. [10] have also presented a skin friction reduction trend as function of the streamwise direction with $Re_\theta = 1190$, $D_m^+ = 350$ and $T^+ = 185$. They found that some of the drag reduction effect is still detected at a location of 2δ downstream of the plate, but no information is provided about the distance at which the boundary layer recovers its standard character. Another discrepancy is drag reduction measured at $x/\delta = -1.5$, whereas our data suggest that no influence upstream of the moving plate occurs.

Aside from data by Trujillo et al. [9], Laadhari et al. [8] also show a value of $\sim 25\%$ for experimental conditions quite comparable with the present ones: $T^+ = 83$, $D_m^+ = 320$ and $Re_\theta = 950$. Results for cylindrical pipe flows at similar operating conditions by Choi and Graham [11] ($\sim$23% drag reduction for $T^+ = 60$, $W_m^+ = 11$) and by Nikitin [4] ($\sim$25% drag reduction for $T^+ = 65$, $W_m^+ = 13$) indicate that the geometry of the system, either planar or cylindrical, does not remarkably influence its drag-reducing properties. This theory has been recently supported by Choi et al. [5], who showed very similar values for turbulent channel and pipe flow geometries. Drag reduction data presented by other researchers at similar W_m (for example [3,7]) are of the order of 40% due to periods of oscillation close to the optimal value ($T^+ \approx 120$).

3.2. Velocity measurements along the vertical direction

This section describes the velocity measurements conducted in the standard and perturbed boundary layers at a downstream location from the foremost edge of the plate of $x/\delta = 6.4$. At this position on the moving section, the Reynolds number was $Re_\theta = 1400$ for the fixed-wall case and the oscillating conditions were given by $D_m^+ = 240$ with $T^+ = 83$ and 42, corresponding respectively to $W_m^+ = 9$ and 18.

After applying the correction detailed in Section 2.4, the values of friction velocity in the oscillating cases were estimated by means of formula 4 with the data of the two closest points to the wall, respectively located at $y_1 = 0.53$ mm and at $y_2 = 0.58$ mm ($y_1^+ = 3.8$ and $y_2^+ = 4.2$ for $W_m^+ = 9$ and $y_1^+ = 3.6$ and $y_2^+ = 3.9$ for $W_m^+ = 18$). The values were $u_{\tau,o} = 0.0072$ and 0.00685 m/s.

The mean streamwise velocity profiles normalized with u_τ are displayed in Fig. 4. The fixed-wall profile compares reasonably well with both the linear relationship in the very near-wall region:

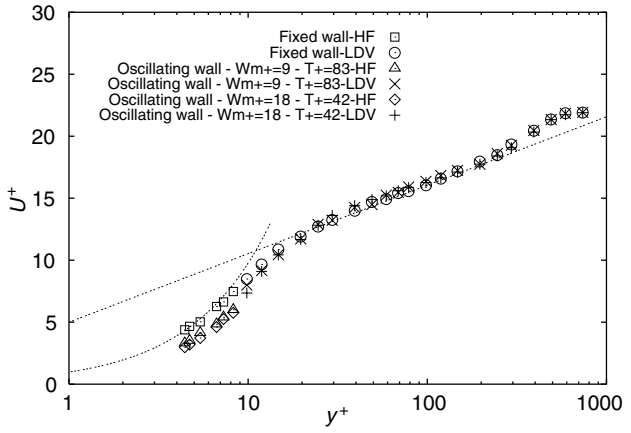

Fig. 4. Mean streamwise velocity profiles at a streamwise location of $x/\delta = 6.4$ scaled with u_τ. The symbols are adopted from the present figure through Fig. 12. The near wall curve is Eq. (5) and the straight line indicates the "log-law" given by Eq. (2).

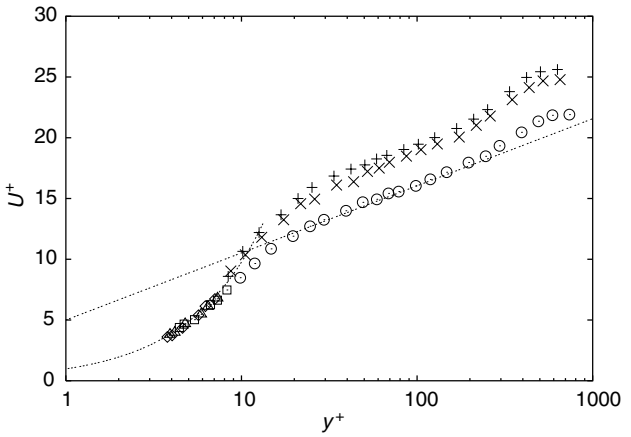

Fig. 5. Mean streamwise velocity profiles at a streamwise location of $x/\delta = 6.4$ scaled with $u_{\tau,o}$.

$$U^+ = y^+, \tag{5}$$

and with the logarithmic law of the wall (Eq. (2)). The oscillating-wall trends present a decrease compared to the fixed-wall profile for $0 < y^+ < 20$, and 25% drag reduction is observed for $W_m^+ = 9$ and 32% for $W_m^+ = 18$. These two values of drag reduction seem to compare well with the interpolation of the highly accurate DNS results of channel flow by Ricco and Quadrio [7]. The reduction in mean velocity vanishes when $y^+ > 30$ for both oscillating cases. A slight upward shift of the velocity profile in the logarithmic-law region acts to balance the velocity deficit for $y^+ < 30$ to conserve the mass flux. This change has also been observed by Jung et al. [1] and Laadhari et al. [8].

The mean velocity profiles scaled with $u_{\tau,o}$ are presented in Fig. 5. The velocity data collapse on a single trend for $y^+ < 10$ and the profiles for the oscillating cases are shifted upward in the remaining portion of the boundary layer. This result is characteristic of drag reducing flows, as shown by Choi [29], and analogous to the downward shift of the mean velocity profiles occurring for rough surface flows, which present an increase in skin friction coefficient.

The u' profiles are plotted in Figs. 6 and 7, respectively for scaling with u_τ and $u_{\tau,o}$. The data show a similar decrease up to the logarithmic-law region, whereas no influence is observed for $y^+ > 200$. The peak for the two profiles is reduced by the same amount ($\sim 14\%$) and shifts upward at a location of $y^+ \approx 25$, whereas the peak of the fixed-wall profile is at $y^+ \approx 15$. The peak of u' reduces by $\sim 20\%$ and moves to higher positions also according to other studies [1,2,8,9].

The behavior of u' scaled with $u_{\tau,o}$ is shown in Fig. 7. The oscillating profiles show lower values than the stationary profile for location of $y^+ < 20$, whereas no remarkable differences are notable in the remaining part

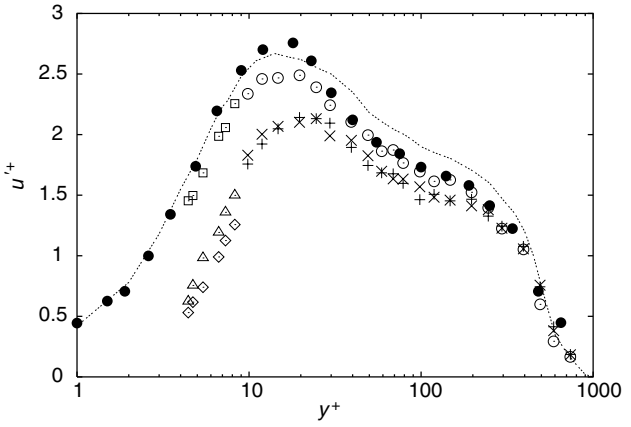

Fig. 6. R.m.s streamwise velocity profiles at a streamwise location of $x/\delta = 6.4$ scaled with u_τ. The line indicates data by Spalart [24] and full circles denote data by DeGraff and Eaton [25].

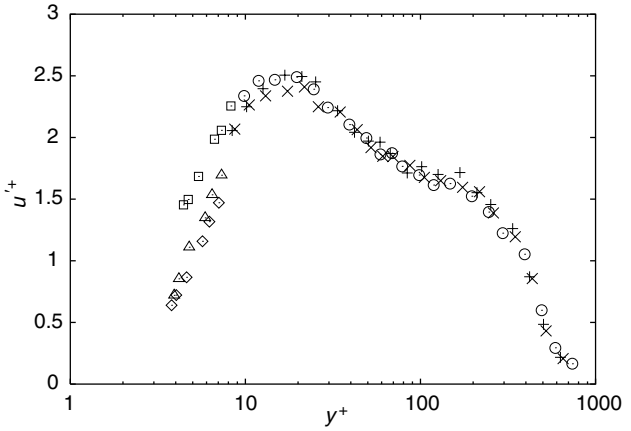

Fig. 7. R.m.s streamwise velocity profiles at a streamwise location of $x/\delta = 6.4$ scaled with $u_{\tau,o}$.

of the boundary layer. Profiles now collapse in the logarithmic-law region of the boundary layer in as much as

they scale with u_τ, which is lower in the oscillating cases. Here the result of oscillations is felt indirectly: the direct effect of the oscillations is confined in the proximity of the wall, whereas the change in u_τ is passively felt in the logarithmic-law region. The pattern is a clear indication that the reduction in fluctuations near the wall is proportionally greater than the reduction of the mean values. The scaling with $u_{\tau,o}$ reveals that the wall oscillation besides reducing the wall stress and thus the Reynolds number, significantly alters the character of the flow up to the buffer region.

Fig. 8 pictures the v' profiles normalized with u_τ. Both oscillating cases cause a decrease in the fluctuations: the case with lower W_m extends its influence up to $y^+ \approx 300$, whilst slightly lower values for $y^+ < 30$ are detected when $W_m^+ = 18$. Similarly to u', the maximum values are shifted upward at a location of $y^+ \approx 200$, whereas the maximum v'^+ in the fixed-wall case is at $y^+ \approx 100$. These profiles match very well the ones in [2,3,8,9].

The turbulence shear stresses $-\overline{uv}$ are non-dimensionalized with u_τ^2 and plotted in Fig. 9. Both oscillating cases present consistent reductions up to $y^+ \approx 200$ and very similar trends throughout the boundary layer. The peak in the fixed-wall configuration reduces by $\sim 25\%$ when the oscillations are imposed and shifts upward from $y^+ \approx 70$ to ≈ 200 for both perturbed cases. The Reynolds stresses are attenuated more than the single u and v fluctuations, indicating that the oscillation not only acts as a turbulence attenuator, but also that the dynamical link of the turbulent structures might be greatly disrupted. Data by Trujillo et al. [9] match well the present ones, showing a peak reduction of $\sim 20\%$ and the uniform pattern in the logarithmic-law region. Results in [1,3,8] also show comparable reductions of the maximum Reynolds stress. Only Dhanak and Si [16] show a Reynolds stress decrement significantly higher than the computed amount of drag reduction ($\sim 60\%$ and $\sim 10\%$, respectively).

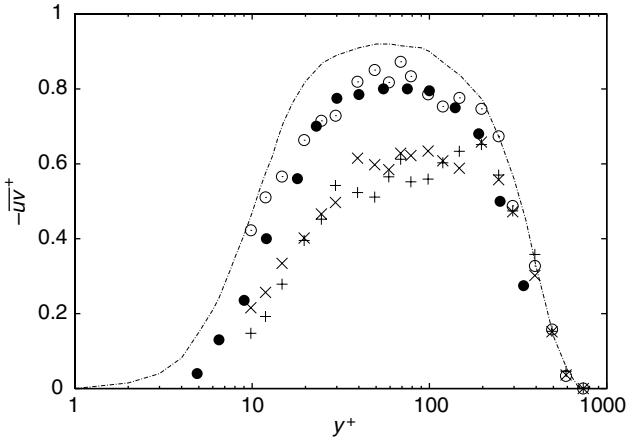

Fig. 9. Reynolds stresses profile at a streamwise location of $x/\delta = 6.4$ scaled with u_τ. The line indicates data by Spalart [24] and full circles denote data by DeGraff and Eaton [25].

A 10% decrease in $-R_{uv}$ is visible in the logarithmic-law region (see Fig. 10). The values are even lower in the buffer region ($\sim 25\%$ at $y^+ = 10$ for the high-W_m case) and seem to diminish even more moving closer to the wall. This behavior is an indication of the more intense reduction of the Reynolds stresses than of the product of the single r.m.s fluctuations. Not only the fluctuations are diminished, but the coherence between the two velocity component is weakened by the action of wall. Interestingly, the region dominated by the Stokes layer, ($0 < y^+ < \delta_s^+$; $\delta_s^+ = \sqrt{4\pi T^+} = 23$ for $T^+ = 42$ and $\delta_s^+ = 32$ for $T^+ = 83$) corresponds to the part of the boundary layer where the correlation coefficient is reduced the most, whereas smaller decrements occur for $30 < y^+ < 500$. It is then evident that the spanwise frictional layer interferes with the turbulence-producing cycle and is responsible for the modification of the near-wall turbulence dynamics, for example by thickening the viscous sublayer [2]. Indeed, as pointed out by Quadrio and Sibilla [3] and visualized by Quadrio and Ricco [6],

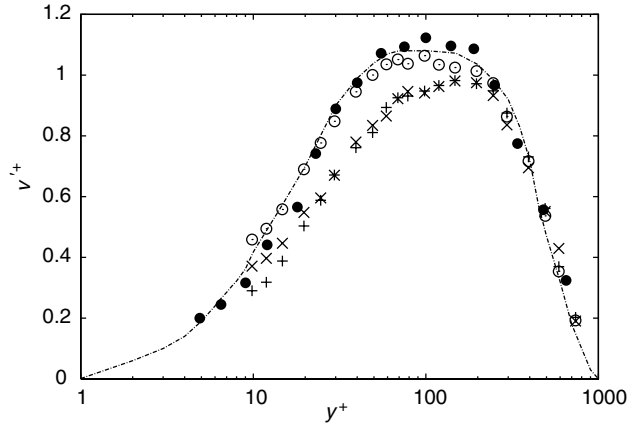

Fig. 8. R.m.s vertical velocity profiles at a streamwise location of $x/\delta = 6.4$ scaled with u_τ. The line indicates data by Spalart [24] and full circles denote data by DeGraff and Eaton [25].

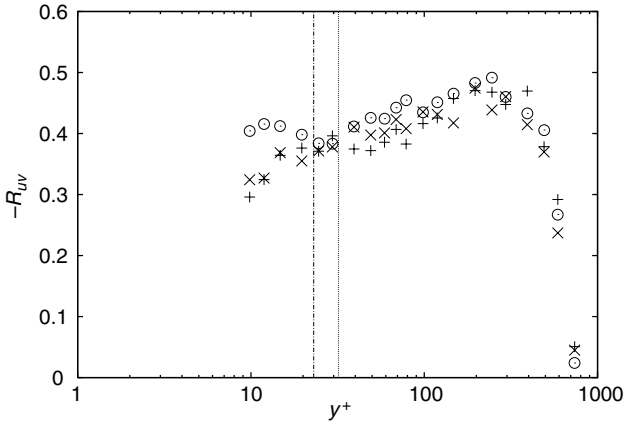

Fig. 10. Correlation coefficient profiles at a streamwise location of $x/\delta = 6.4$. Straight lines indicate thicknesses of Stokes layer δ_s^+ for $T^+ = 42$ and $T^+ = 83$.

the maximum effect of drag reduction accrues when the low-speed pockets are well merged in the near-wall region where spanwise shear stresses are significant.

In order to understand better the phenomena occurring in the forced boundary layer, the production and transport terms of turbulent kinetic energy (TKE) are investigated. The TKE production $-\overline{uv}^+\partial U^+/\partial y^+$ by Reynolds stress transport are plotted using v/u_τ^4 for normalization and displayed in Fig. 11. The wall oscillation inhibits the TKE production up to $y^+ \approx 200$ and the peak decreases of $\sim 25\%$ in the low-W_m case and of $\sim 50\%$ for the high-W_m case. These results are consistent with the reduction of the turbulent intensities and of the Reynolds stresses up to the logarithmic-law region and confirm the idea that the sinusoidal motion of the wall significantly damps the turbulence activities. Previous numerical simulations [2,6,16] and one experimental investigation [30] present similar behaviors of TKE production as function of y^+. Fig. 12 shows that the TKE transport term $\partial(-\overline{uv}^+U^+)/\partial y^+$ is also strongly weakened by the wall motion and the maximum value is reduced by $\sim 40\%$.

3.3. Reynolds number effect on drag reduction

The influence of the Reynolds number on the amount of drag reduction is investigated. For each Reynolds number, namely $Re_\theta = 500$, 950 and 1400, the lateral excursion was kept fixed and the values of D_m were very similar for the three cases, i.e. $D_m^+ \approx 200$, 240 and 240, respectively, thus allowing a valuable comparison amongst the drag reduction data. Since the experimental setup only permitted varying the spanwise wall displacement for four cases, the above-mentioned oscillatory conditions were chosen in order to obtain similar non-dimensional values for D_m.

Fig. 13 presents the values of skin-friction reduction as function of T^+, where the abscissa is shown in logarithmic scale for clarity. It appears that there is no

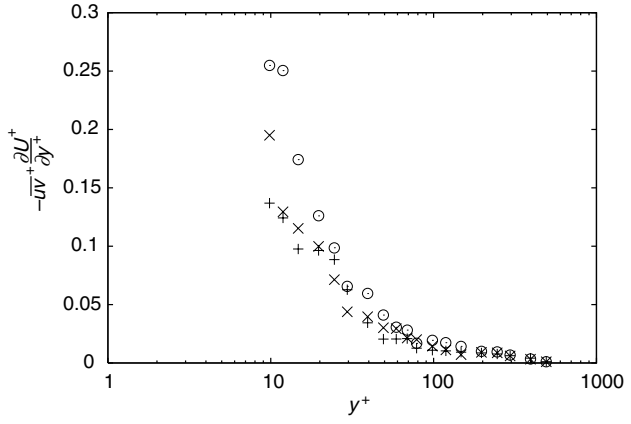

Fig. 11. Production of turbulent kinetic energy at a streamwise location of $x/\delta = 6.4$ scaled with u_τ.

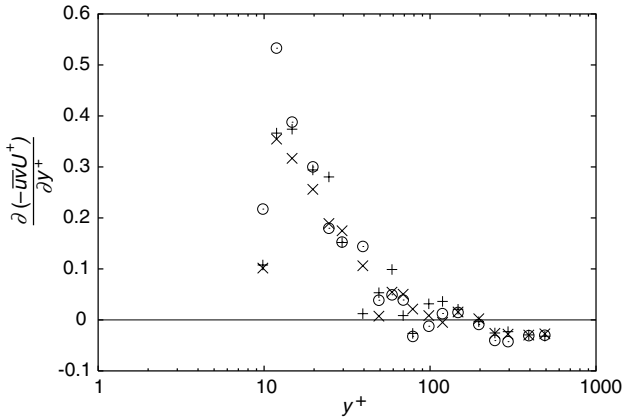

Fig. 12. Transport of mean kinetic energy by Reynolds stresses at a streamwise location of $x/\delta = 6.4$ scaled with u_τ.

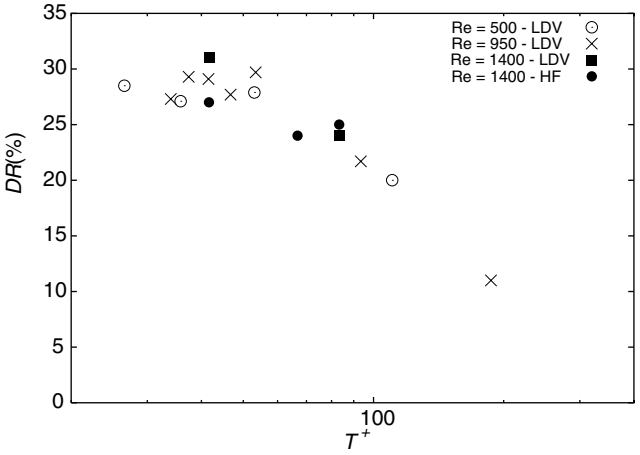

Fig. 13. Drag reduction as function of T^+ for different Re_θ.

dramatic effect of Reynolds number on the drag reduction properties for the conditions tested. The present measurements are now compared with data by other researchers with similar values of D, and we observe that our finding is in line with most of the previous investigations as shown in Fig. 14. In agreement with our results, the pipe-flow investigation by Choi and Graham [11] shows that the differences of the amounts of drag reduction due to the Reynolds number variation for similar values of T and D_m are within the uncertainty range of the measurements. Data by Trujillo et al. [9] at $Re_\theta = 1500$ and by Choi and Graham [11] at $Re_\tau = 530$ are similar to each other and lower than the present ones, probably on account of the bias due to the spanwise component of velocity. DNS results by Quadrio and Sibilla [3] and Ricco and Quadrio [7] both at $Re_\tau = 200$ appear consistent with themselves and slightly higher than the present ones for $60 < T^+ < 120$. On the contrary, the numerical analysis by Choi et al. [5] outlines a strong dependence of the drag-reducing properties on the Reynolds number. They found that

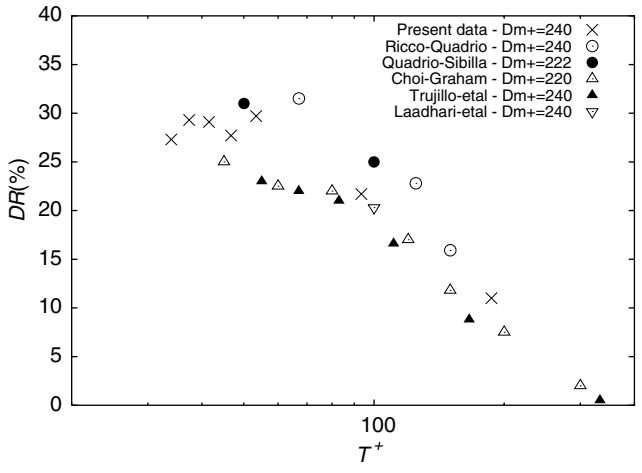

Fig. 14. Comparison of present data at $Re_\theta = 950$ with data by other investigators.

increasing the non-dimensional parameter by four times from $Re_\tau = 100$ to 400 can halve the amount of drag reduction, for $T^+ \leqslant 50$ and W_m^+ as high as 20. This controversy therefore identifies the issue of the Reynolds number dependence as an interesting open point of discussion.

It emerges that the energy-saving effect of the oscillation strongly depends on T for fixed displacement D_m, increasing as T decreases up to $T^+ = 40$–50. Drag reduction is low for high T for the Stokes layer thickness not only moves the low-speed streaks laterally, but also starts affecting the longitudinal vortices so that the disruption between these coherent structures is not effective. As also pointed out by Baron and Quadrio [2], the amount of drag reduction is expected to diminish to zero as $T \to 0$ since δ_s vanishes and the near-wall structures are then not influenced by the oscillation. It was not however possible to perform measurements at lower periods to confirm this idea due to limitations of the mechanical system. Nonetheless, it appears that the optimum T for fixed D_m is lower that the optimum T for fixed W_m (which is $T^+ \approx 120$ and does not depends on W_m, as verified by Quadrio and Sibilla [3] and by Ricco and Quadrio [7]).

4. Conclusions

The present work confirms previous experimental and numerical results and further investigates the modifications on a turbulent boundary layer given by spanwise wall oscillations.

Velocity measurements have been conducted by LDV and hot-film anemometer to meet these purposes. Streamwise mean velocity profiles for the oscillating cases show a decrease in mean streamwise velocity in the viscous sublayer and in the buffer region up to $y^+ \approx 30$. The lower mean velocity gradient in the streamwise direction point out the expected reduction in wall-shear stress and the highest drag reduction of 32% is attained for oscillating conditions of $W_m^+ = 18$, $T^+ = 42$ and $Re_\theta = 1400$. All the statistical parameters, such as u', v', $-\overline{uv}$, and R_{uv} are shifted upward by an amount comparable to the thickness of the Stokes layer and are strongly reduced as an indication of the taming effect on turbulence established by the wall motion.

The behavior of drag reduction along the streamwise coordinate has been studied. The effect starts at the foremost edge of the plate and reaches the maximum value at a location of $\sim 3\delta$ where it seems to level off to $\sim 23\%$ (for conditions of $T^+ = 67$ and $W_m^+ = 11.3$). The influence decays exponentially downstream of the moving surface, diminishing to 5% at $\sim 1\delta$ from the rearmost edge and disappearing at a distance of $\sim 2\delta$.

The relevant issue of the dependence of drag reduction on the Reynolds number has been addressed and we discern that the skin friction attenuation is not influenced by the variation of the non-dimensional parameter, for $Re_\theta \leqslant 1400$.

Acknowledgements

The authors wish to thank Dr. Maurizio Quadrio for proofreading a preliminary version of the manuscript and for providing insightful comments and Dr. Trujillo and Prof. Bogard for guidance during the experimental analysis.

References

[1] W.J. Jung, N. Mangiavacchi, R. Akhavan, Suppression of turbulence in wall-bounded flows by high-frequency spanwise oscillations, Physics of Fluids A 4 (8) (1992) 1605–1607.
[2] A. Baron, M. Quadrio, Turbulent drag reduction by spanwise wall oscillations, Applied Scientific Research 55 (1996) 311–326.
[3] M. Quadrio, S. Sibilla, Numerical simulation of turbulent flow in a pipe oscillating around its axis, Journal of Fluid Mechanics 424 (2000) 217–241.
[4] N.V. Nikitin, On the mechanism of turbulence suppression by spanwise surface oscillations, Fluid Dynamics 35 (2) (2000) 185–190.
[5] J.-I. Choi, C.-X. Xu, H.J. Sung, Drag reduction by spanwise wall oscillation in wall-bounded turbulent flows, AIAA Journal 40 (5) (2002) 842–850.
[6] M. Quadrio, P. Ricco, Initial response of a turbulent channel flow to spanwise oscillation of the walls, Journal of Turbulence 4 (7) (2003).
[7] P. Ricco, M. Quadrio, Turbulent drag reduction over an oscillating wall, in: 5th Euromech Fluid Mechanics Conference, Toulouse, France, August 24–28, 2003.
[8] F. Laadhari, L. Skandaji, R.M. Morel, Turbulence reduction in a boundary layer by local spanwise oscillating surface, Physics of Fluids 6 (10) (1994) 3218–3220.

[9] S.M. Trujillo, D.G. Bogard, K.S. Ball, Turbulent boundary layer drag reduction using an oscillating wall, AIAA Paper 97-1870, 1997.
[10] K.-S. Choi, J.R. DeBisschop, B.R. Clayton, Turbulent boundary-layer control by means of spanwise-wall oscillation, AIAA Journal 36 (7) (1998) 1157–1162.
[11] K.-S. Choi, M. Graham, Drag reduction of turbulent pipe flows by circular-wall oscillation, Physics of Fluids 10 (1) (1998) 7.
[12] K.-S. Choi, Near-wall structure of turbulent boundary layer with spanwise-wall oscillation, Physics of Fluids 14 (7) (2002) 2530–2542.
[13] G.E. Karniadakis, K.-S. Choi, Mechanisms on transverse motions in turbulent wall flows, Annual Review of Fluid Mechanics 35 (2003) 45–62.
[14] Y. Du, V. Symeonidis, G.E. Karniadakis, Drag reduction in wall-bounded turbulence via a transverse travelling wave, Journal of Fluid Mechanics 457 (2002) 1–34.
[15] D.W. Bechert, M. Bruse, W. Hagel, J.G.T. van der Höven, G. Hoppe, Experiments on drag reducing surfaces and their optimization with an adjustable geometry, Journal of Fluid Mechanics 338 (1997) 59–87.
[16] M.R. Dhanak, C. Si, On reduction of turbulent wall friction through spanwise oscillations, Journal of Fluid Mechanics 383 (1999) 175–195.
[17] T.W. Berger, J. Kim, C. Lee, J. Lim, Turbulent boundary layer control utilizing the Lorentz force, Physics of Fluids 12 (3) (2000) 631–649.
[18] M.T. Coughran, Interdependence of large and small structures in a turbulent boundary layer, PhD Dissertation, The University of Texas at Austin, 1998.
[19] C.T. Lomas, Fundamentals of Hot Wire Anemometry, Cambridge University Press, 1986.
[20] H.H. Bruun, Hot-film anemometry in liquid flows, Measurement Science and Technology 7 (1996) 1301–1312.
[21] B.C. Khoo, Y.T. Chew, C.J. Teo, Near-wall hot-wire measurements—Part II: Turbulence time scale, convective velocity and spectra in the viscous sublayer, Experiments in Fluids 31 (2001) 494–505.
[22] S.B. Pope, Turbulent Flows, Cambridge University Press, 2000.
[23] F. Durst, H. Kikura, I. Lekakis, J. Jovanovic, Q. Ye, Wall shear stress determination from near-wall mean velocity data in turbulent pipe and channel flows, Experiments in Fluids 20 (1996) 417.
[24] P.R. Spalart, Direct simulation of a turbulent boundary layer up to $Re_\theta = 1410$, Journal of Fluid Mechanics 187 (1988) 61–98.
[25] D.B. DeGraff, J.K. Eaton, Reynolds-number scaling of the flat-plate turbulent boundary layer, Journal of Fluid Mechanics 422 (2000) 319.
[26] W.M. Kays, M.E. Crawford, Convective Heat and Mass Transfer, third ed., McGraw-Hill, 1993, p. 208.
[27] P. Ligrani, Measurements techniques, VKI for Fluid Dynamics—Course note 108—Rhode Saint Genese Belgium, 1979.
[28] K.-S. Choi, B.R. Clayton, The mechanism of turbulent drag reduction with wall oscillation, International Journal of Heat and Fluid Flow 22 (2001) 1–9.
[29] K.-S. Choi, Near-wall structure of a turbulent boundary layer with riblets, Journal of Fluid Mechanics 208 (1989) 417–458.
[30] G.M. Di Cicca, G. Iuso, P.G. Spazzini, M. Onorato, Particle image velocimetry investigation of a turbulent boundary layer manipulated by spanwise oscillations, Journal of Fluid Mechanics 467 (2002) 41–56.